Cell geometry and leaflet bilayer asymmetry regulate domain formation in plasma membranes

Md Zulfikar Ali,[1] Kerwyn Casey Huang,[2,3,4] Ned S. Wingreen,[5] and Ranjan Mukhopadhyay[1,*]

[1]*Department of Physics, Clark University, Worcester, Massachusetts 01610, USA*

[2]*Department of Bioengineering, Stanford University, Stanford, California 94305, USA*

[3]*Department of Microbiology and Immunology, Stanford University School of Medicine, Stanford, California 94305, USA*

[4]*Chan Zuckerberg Biohub, San Francisco, California 943158, USA*

[5]*Department of Molecular Biology, Princeton University, Princeton, New Jersey 08540, USA*

(Received 23 June 2017; revised manuscript received 19 November 2018; published 2 January 2019)

We model how pattern formation in a multicomponent lipid bilayer pinned to an elastic substrate is governed by the interplay between lipid phase separation and the tendency of domains of high intrinsic curvature lipids to deform the membrane away from a stiff substrate such as the cell wall. The emergent patterns, which include compact and striped lipid microdomains, are anticorrelated across the two leaflets and depend on leaflet asymmetry, the ability of lipids to flip between leaflets, and the global geometry. We characterize analytically the dependence of stripe width on lipid parameters, and consider the implications of interleaflet patterning for curvature-dependent lipid localization.

DOI: 10.1103/PhysRevE.99.012401

I. INTRODUCTION

Recent studies have highlighted the role of biological membranes in subcellular protein organization and protein function [1–7], both in eukaryotic and prokaryotic cells. A growing body of experimental findings and theoretical models has led to the recognition that membrane curvature can guide the spatial organization of lipids and membrane-associated proteins [4], providing a mechanism for localization that emerges directly from cell geometry rather than relying on targeting to other molecules. Moreover, constituent lipids and proteins can then cause membrane deformations that alter the surface landscape. *In vitro* experiments with supported lipid bilayers have demonstrated the influence of molecular shape on membrane curvature and phase separation, linking the biochemical composition and mechanics of membranes (see Ref. [2] for a review). In this paper, we develop a minimal model to study the role of bending-mediated forces in governing spatial patterning at length scales substantially larger than individual molecules. Our model and results provide a deeper understanding of lipid and protein organization in prokaryotic and eukaryotic membranes [1,4,8–14], as well as for *in vitro* supported bilayers [2,15–17]. Moreover, insight into the self-assembly mechanisms of multicomponent membranes will facilitate the design of novel materials whose fabrication transcends traditional constraints.

To study how geometry affects the spatial organization of a multicomponent membrane, we extend a previous model [18,19] that was proposed in the context of localization of the lipid cardiolipin within the cytoplasmic membranes of rod-shaped bacteria such as *Escherichia coli* and *Bacillus subtilis*. Cardiolipin, which has two head groups and four tails and thus a high intrinsic negative curvature, has been shown to localize to the septal and polar regions [8–10], which have slightly higher curvature than the midcell region. We previously argued that due to the large size mismatch between individual lipids (<1 nm) and the cell radius (∼500 nm), the energetics of individual cardiolipin molecules are insufficient to explain the observed preference for the poles, and hence that polar localization likely requires the formation of cardiolipin clusters of intermediate size [18,19]. In a recent study in which *E. coli* cells were reshaped into ellipsoidal molds of different curvatures, domain formation and "polar" localization were observed at a crossover curvature approximating that of normal, rod-shaped cells [11]. Moreover, we suggested that domains of cardiolipin could mediate protein targeting [18,19], which was independently discovered for the osmosensory transporter ProP in *E. coli* [20].

Our previous work considered only the energetics of the inner leaflet of the membrane. However, two factors suggest that the outer leaflet may impact the organization of the inner leaflet. Lipids are able to flip between the leaflets through the activity of flippases, suggesting that energetics may drive changes in the relative composition of each leaflet. Moreover, due to the coupling between composition and curvature in our model, domains in one leaflet can effectively interact with domains in the other leaflet. This in turn could also affect curvature dependent localization, since the preference of a domain of cardiolipin in the inner leaflet for regions of higher curvature could be counterbalanced by the disfavoring of a similar domain in the outer leaflet. In the current study, we consider a two-component bilayer membrane, in which one of the lipid types has a higher intrinsic curvature (e.g., cardiolipin). Coupling of membrane geometry to the shape of the cell is represented by a potential that captures the pinning of the membrane to the external cell wall by turgor pressure in bacteria, and binding to the cortical cytoskeleton in eukaryotic cells. While for model membranes *in vitro* it is typically assumed that the timescale for lipid flipping

*ranjan@clarku.edu

between leaflets is long (several hours) [21,22], the presence of flippases in biological membranes [23] allows the two leaflets to more rapidly equilibrate [23]. Thus, we consider the effect of cardiolipin partitioning into both leaflets of the membrane for two cases: (i) where the lipid composition is separately fixed in each leaflet (no flipping), and (ii) where lipids are allowed to flip between the leaflets. In both cases, we identify a rich phase space of cluster morphologies, some of which have direct connections with experimental observations [24].

II. MODEL

In our model of a pinned two-component lipid bilayer, we consider lipids of type A, with high intrinsic curvature γ, and type B, with zero intrinsic curvature. We allow lipids to be asymmetrically distributed between the two leaflets, and each leaflet can have lipids of both types. The total energy of the membrane is

$$E = E_{\text{elastic}} + E_{\text{int}}^{\text{in}} + E_{\text{int}}^{\text{out}}, \tag{1}$$

where E_{elastic} represents the elastic energy of the membrane and $E_{\text{int}}^{\text{in/out}}$ represents short-range lipid-lipid interactions in the inner and outer leaflet. The elastic energy is a sum of the bending energy of the two leaflets and a pinning potential that penalizes deviation from a preferred height:

$$E_{\text{elastic}} = \int_M \left(\frac{\kappa}{2}\{[2H(\mathbf{r})]^2 + 2[\gamma_{\text{out}}(\mathbf{r}) - \gamma_{\text{in}}(\mathbf{r})]H(\mathbf{r})\} + \frac{\lambda}{2}[h(\mathbf{r}) - h_0(\mathbf{r})]^2 \right) d\mathbf{r}, \tag{2}$$

where the domain of integration M is the two-dimensional surface representing the lipid bilayer [25]; the subscript M will be omitted in all integrals that follow. The last term, proportional to the pinning modulus λ, is the pinning potential that penalizes mid-plane deformations of the membrane away from its minimum-energy position with respect to the substrate (cell wall or cytoskeleton), with $h(\mathbf{r})$ representing the local height of the membrane and $h_0(\mathbf{r})$ the preferred height. In the case of bacteria, this pinning potential represents the coupling of the cytoplasmic membrane to the cell wall, believed to be driven in large part by the turgor pressure, as removing turgor through hyperosmotic shock causes plasmolysis (separation of the membrane from the cell wall) [26]. In eukaryotic cells, this potential represents the coupling or pinning of the membrane to the actin cytoskeleton through diverse interactions [27]. A similar energy term has also been used previously in the literature in the context of deformations of red blood cell membranes coupled to the cytoskeleton [28], although not in the context of bilayer asymmetry, as we have addressed in this manuscript. In Eq. (2), H is the local mean curvature of the two-dimensional membrane, and γ_{in} and $\gamma_{\text{in/out}}$ are the composition-dependent local intrinsic curvature of the inner and outer leaflets, respectively, given by $\gamma_{\text{in/out}}(\mathbf{r}) = \gamma$ or 0 if there is a lipid A or B, respectively, at $\mathbf{r}$ in the inner or outer leaflet. Within each leaflet, the interaction energy represents the energetic contribution from short-range chemical interaction between the lipids, including electrostatic, van der Waals, and hydrophobic interactions. We neglect species-dependence of the inter-leaflet lipid interaction. If we represent the membrane as a two-dimensional lattice, then the interaction energy can be written as a sum of two contributions, $E_{\text{int}}^{\text{in}}$ and $E_{\text{int}}^{\text{out}}$, corresponding to the inner and outer leaflets of the bilayer,

$$E_{\text{int}}^{\text{in/out}} = \sum_{\langle i,j \rangle} \sum_{\alpha,\beta} \phi_{i,\alpha}^{\text{in/out}} \phi_{j,\beta}^{\text{in/out}} \varepsilon_{\alpha\beta}, \tag{3}$$

where $\phi_{i,\alpha}^{\text{in/out}} = 0$ or 1 indicates the absence or presence of the lipid species denoted by α at lattice site i in the inner or outer leaflet, and α can be either A or B. We consider only nearest neighbor interactions $\langle i, j \rangle$, with $\varepsilon_{\alpha\beta}$ being the lipid-lipid interaction energy.

We minimize the energy of this system using a Metropolis Monte Carlo algorithm. We represent the two leaflets as two-dimensional triangular lattices fully occupied by lipids of types A or B (see Appendix C); we previously showed that triangular and square lattices produce similar results [19]. Within each leaflet, we consider only nearest neighbor interactions with strength $\varepsilon_{\alpha\beta}$, where α, β can be either A or B. Unless otherwise specified, the simulations were performed with a 100×100 periodic triangular lattice, the membrane stiffness modulus was $\kappa = 25\, k_{\text{B}}T$ and the pinning modulus was $\lambda = 0.25\, k_{\text{B}}T\ \text{nm}^{-4}$. To simplify the exploration of parameter space, we set $\varepsilon_{\text{AA}} = \varepsilon_{\text{BB}} = 0$ and varied only the repulsive interaction energy ε_{AB} between unlike lipids.

III. PATTERN FORMATION ON A FLAT SUBSTRATE

We first focused on the case of a flat substrate ($h_0 = 0$), and studied pattern formation for relatively low lipid A concentration (7.5% lipid A and 92.5% lipid B) in each leaflet, consistent with the low levels of cardiolipin in *E. coli* and *B. subtilis*. We assumed no lipid flipping between the two leaflets; for flat substrates, flipping simply ensures identical lipid fractions, on average, in both leaflets. For fixed values of κ and λ, we observed robust and characteristic pattern formation for different values of intrinsic curvature γ and interaction energy ε_{AB}. For high values of $\varepsilon_{\text{AB}} = 1\, k_{\text{B}}T$ and low $\gamma = 0.2\ \text{nm}^{-1}$, bending and pinning were relatively minor contributions to the total energy and the membrane minimized its energy by forming single large domains of lipid A in each leaflet [Fig. 1(a)]. These domains were never observed to overlap across the two leaflets. For larger γ, we observed striped domains of lipid A that alternated in space between the leaflets [Fig. 1(b)]. The stripe width was determined by the values of γ and ε_{AB}, with larger γ resulting in decreased stripe width [Fig. 1(c)]; we will analyze, in detail, the dependence of stripe width on model parameters in the next section. For asymmetric lipid compositions with higher lipid A fraction in the inner leaflet, we observed the coexistence of striped domains and smaller lipid A microdomains in the inner leaflet [Fig. 1(d)].

The local concentration of lipid A was much higher within the region of striped domains (around 50% in each leaflet). Consequently, to explore the physics of stripe formation, we studied membranes with higher fractions of lipid A in each leaflet. To investigate the effects of asymmetric composition on pattern formation, we maintained a constant total amount of lipid A and lipid B (50% of each), but allowed for unequal partitioning between the two leaflets. The fraction of lipid A

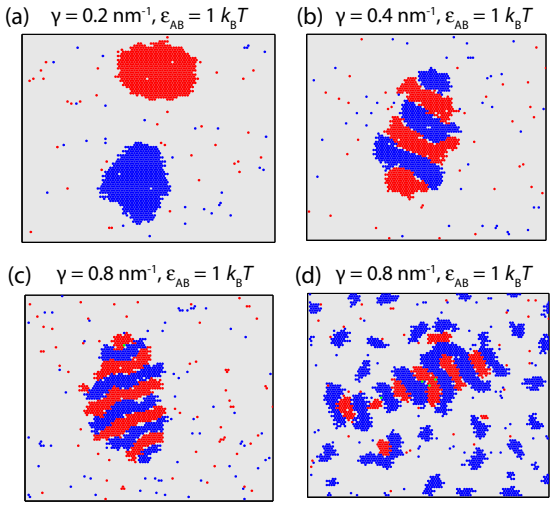

FIG. 1. Lipids in a two-component membrane can form domains or stripes depending on the intrinsic curvature of the lipids. Shown are typical membrane configurations from simulations of a flat cell surface in the absence of lipid flipping between the leaflets. Blue (dark gray, in print) and red (intermediate gray, in print) represent lipid A locations solely in the inner and outer leaflet, respectively; light gray (green) represents locations occupied by lipid B (lipid A) in both leaflets. (a–c) For equal lipid A fractions $\phi_{in} = \phi_{out} = 0.075$ in the two leaflets, increasing γ leads to a transition from a single domain to stripes with width inversely proportional to γ. (d) For asymmetric composition $\phi_{in} = 0.2$ and $\phi_{out} = 0.05$, a combination of stripes and microdomains occurs.

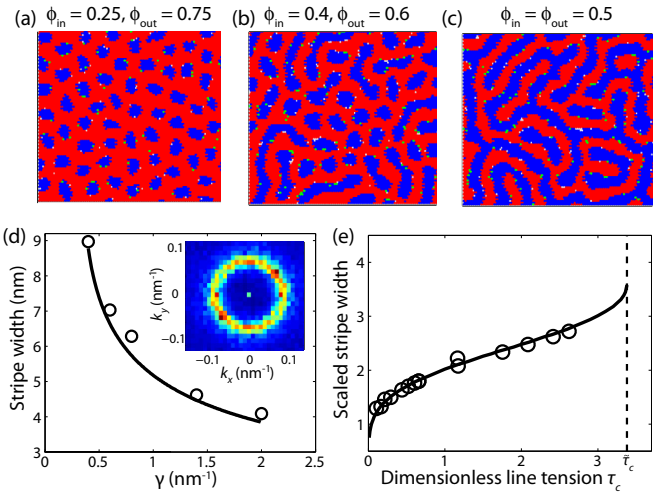

FIG. 2. Transition from microdomains to stripe formation as leaflet asymmetry is reduced. The total amounts of lipid A and B are held fixed, while partitioning between the leaflets is varied. (a–c) Increasing lipid A fraction in the inner leaflet, for fixed intrinsic curvature γ. For subfigure (a), $\phi_{in} = 0.25$ and $\phi_{out} = 0.75$, for (b) $\phi_{in} = 0.4$ and $\phi_{out} = 0.6$, and for (c) $\phi_{in} = \phi_{out} = 0.5$. As in the previous figure, blue (dark gray, in print) and red (intermediate gray, in print) represent lipid A located solely in the inner and outer leaflet, respectively, while light gray (green) represents regions occupied by lipid B (lipid A) in both leaflets. (d) Stripe width as a function of γ, estimated from the Fourier transform of the configuration of lipid A molecules (circles) and estimated from our analytical calculation (solid curve). Inset: Fourier transform from a simulation with parameters of (c). The stripe width is inversely proportional to the radius of the ring in Fourier space. (e) Variation of scaled stripe width from simulation (circles) and calculated analytically (curve) for line tension $\tau = 1.68\, k_B T \mathrm{nm}^{-1}$.

in each leaflet had a strong influence on the resulting pattern (Fig. 2). For a high degree of asymmetry (lipid A fractions $\phi_{in} = 0.25$ and $\phi_{out} = 0.75$), simulations produced regularly spaced, approximately circular microdomains arranged in a roughly hexagonal pattern [Fig. 2(a)]. For a smaller degree of asymmetry ($\phi_{in} = 0.4$, $\phi_{out} = 0.6$), we observed a mixture of stripes and compact domains [Fig. 2(b)], while for symmetric leaflets ($\phi_{in} = \phi_{out} = 0.5$), we obtained stripes covering the entire membrane [Fig. 2(c)]. We can measure the average stripe width from the Fourier transform of the lipid composition [Fig. 2(d), inset]. This transition from a hexagonal array of domains at higher compositional asymmetry to a striped pattern for symmetric leaflet composition is consistent with recent studies of multicomponent vesicles [29,30].

IV. PHYSICS OF STRIPE FORMATION

What drives stripe formation in these two-component membranes? The general notion is that microdomains/stripes arise due to the competition between interaction-driven phase separation and the tendency of lipid domains with high intrinsic curvature to deform the membrane away from its preferred height, which results in a higher elastic energy penalty for larger lipid A domains due to the pinning potential. Based on this idea, we expect smaller domains or thinner stripes for higher values of the intrinsic curvature γ or of the pinning modulus λ. We estimated the average stripe width from the Fourier transform of the lipid composition [Fig. 2(d), inset], and indeed stripe width varied inversely with γ [Fig. 2(d), Fig. 6]. From a complementary perspective, we previously demonstrated that the elastic membrane energetics result in an effective long-range repulsive interaction between two lipid A molecules in the same leaflet [19]. Extending that notion, we find that two lipid A molecules in *different* leaflets experience a similar effective long-range interaction that is now attractive (Appendix A), except when their lateral positions overlap. For the case where the two lipid A molecules in different leaflets are present at the same lateral membrane position there is an elastic energy cost that arises due to frustration of the preferred curvature for each leaflet. As a result, lipid A domains in different leaflets attract each other but have an energy penalty for direct overlap. It is this effective elastic interaction that gives rise to the formation of domains or stripes, and also explains the transition from stripes to compact domains with varying lipid partition between the two leaflets.

To convert this physical intuition into an analytical calculation of stripe width, we assume for simplicity that the stripes are rectangles of width w_s that alternate between the two leaflets. We define a line tension τ at the interface of the stripe domain of the two unlike lipids. This line tension arises from the curvature mismatch at the interface as well as the interaction energy between the unlike lipids; while in our calculation τ will be a fitting parameter, we estimate it to be

of the order of ϵ_{AB}/a, where a is the lattice spacing. For the analysis of stripe formation on a flat substrate, we set $\gamma_0 = 0$, and introduce the fields $\phi(\mathbf{r})^{\text{in/out}}$ that represent the locally averaged fraction of lipid A at position $\mathbf{r}$ in the inner/outer leaflets. Defining $\phi(\mathbf{r}) = \phi(\mathbf{r})^{\text{in}} - \phi(\mathbf{r})^{\text{out}}$, we have $\langle \gamma_{\text{out}}(\mathbf{r}) - \gamma_{\text{in}}(\mathbf{r})\rangle_{\text{local}} = \gamma\phi(\mathbf{r})$. If we substitute $h - h_0$ in Eq. (2) by h, and use the Monge representation, so that for small $\nabla h(\mathbf{r})$ the total mean curvature H can be approximated as $\nabla^2 h/2$, then we can rewrite E_{elastic} in Fourier space as (see Appendix A for details)

$$E_{\text{elastic}} = \int \frac{1}{(2\pi)^2}\left\{(\kappa q^4 + \lambda)\left|h_{\text{q}} + \frac{\kappa\gamma q^2}{2(\lambda + \kappa q^4)}\phi_{\text{q}}\right|^2 - \frac{\kappa^2\gamma^2 q^4}{4(\lambda + \kappa q^4)}|\phi_{\text{q}}|^2\right\} d\mathbf{q}, \tag{4}$$

where h_{q} and ϕ_{q} are the Fourier transforms of $h(\mathbf{r})$ and $\phi(\mathbf{r})$, respectively. We can write down a corresponding thermodynamic partition function,

$$Z_{\text{elastic}} = \text{Tr}_{h,\phi} e^{-E_{\text{elastic}}/k_B T}. \tag{5}$$

First, we carry out the trace over $\{h\}$ (corresponding to integrating over $h_{\mathbf{q}}$ for each value of $\mathbf{q}$) and obtain an effective Hamiltonian purely as a functional of ϕ_q. Carrying out the trace over $\{h\}$ and dropping the constant terms further simplifies Eq. (4) to

$$E_{\text{elastic}} = \frac{\kappa\lambda\gamma^2}{8}\int \frac{1}{(2\pi)^2}\frac{1}{\lambda + \kappa q^4}|\phi_q|^2 d\mathbf{q}. \tag{6}$$

For a membrane with perfect stripes parallel to the vertical axis, $\phi(\mathbf{r})$ depends only on the coordinate x and is periodic with period $2w_s$, and hence can be written as $\phi(\mathbf{r}) = \phi(x) = 1$ (for $0 < x < w_s$, conical lipids in the outer leaflet) or -1 (for $w_s < x < 2w_s$, conical lipids in the inner leaflet). For our calculation, we assume the membrane has dimensions L_x and L_y, where we will take the thermodynamic limit $L_x, L_y \to \infty$. The Fourier series expansion of $\phi(x)$ is $\frac{4}{\pi}\sum_{n=\text{odd}} \sin(n\pi x/w_s)/n$ and the corresponding Fourier transform is given by

$$\phi_q = \int \phi(\mathbf{r}) e^{-i\mathbf{q}\cdot\mathbf{r}} d\mathbf{r} = 8\pi\delta(q_y)\sum_{n=\text{odd}} \frac{i}{n}\left[\delta\left(q_x - \frac{n\pi}{w_s}\right) - \delta\left(q_x + \frac{n\pi}{w_s}\right)\right].$$

Substituting ϕ_q into Eq. (6), and carrying out the integration leads to an elastic energy per unit area of membrane (see Appendix B),

$$\frac{E_{\text{elastic}}}{A} = \frac{\lambda\gamma^2}{\pi^2}\sum_{n=\text{odd}} \frac{w_s^4}{\frac{\lambda}{\kappa}w_s^4 + (n\pi)^4}\frac{1}{n^2}, \tag{7}$$

where $A = L_x L_y$ is the area of the membrane. The energy per unit area due to line tension (τ) for the system is given by

$$\frac{E_{\text{int}}}{A} = \frac{4\tau L_y}{L_y 2w_s} = \frac{2\tau}{w_s}. \tag{8}$$

The total energy per unit area for the system thus can be written as

$$E = \frac{\lambda\gamma^2}{\pi^2}\sum_{n=\text{odd}} \frac{w_s^4}{\frac{\lambda}{\kappa}w_s^4 + (n\pi)^4}\frac{1}{n^2} + \frac{2\tau}{w_s}. \tag{9}$$

For a particular set of parameters, the stripe width can be calculated by minimizing Eq. (7) with respect to w_s. We estimated the value of τ by performing a least-squares fit of the stripe width obtained from our simulations for different values of γ [Fig. 2(d)], yielding $\tau = 1.68\, k_B T$ nm^{-1}, which is of the order of $\epsilon_{AB}/a = 1\, k_B T$ nm^{-1}, consistent with our expectation. For the same value of line tension, we found good agreement between stripe widths obtained from our analytic calculation and from simulations across different pinning moduli (see Appendices B and D). We note that while membrane lipid stripes have been observed previously both experimentally and in simulations [24,29–31], to the best of our knowledge this study represents the first theoretical analysis of stripe formation for lipid bilayers within an equilibrium context.

We can further simplify the calculation by substituting $\alpha = (\kappa/\lambda)^{1/4}$ into Eq. (7), resulting in

$$\tilde{E} = \sum_{n=\text{odd}} \frac{\tilde{w}_s^4}{\tilde{w}_s^4 + (n\pi)^4}\frac{1}{n^2} + \frac{\tilde{\tau}}{\tilde{w}_s}, \tag{10}$$

where $\tilde{E} = \pi^2 E/\kappa\gamma^2$, $\tilde{w}_s = w_s/\alpha$, and $\tilde{\tau} = 2\pi^2\tau/\alpha\kappa\gamma^2$ are dimensionless energy, stripe width, and line tension, respectively. For a given value of $\tilde{\tau}$, the scaled stripe width can be obtained by minimizing the scaled energy $\tilde{E}$. Thus, the scaled stripe width $\tilde{w}_s$ depends only on a single parameter, namely the scaled line tension $\tilde{\tau}$, with simulations in good agreement [Fig. 2(e)]. Moreover, we found that stripes are only stable/metastable for $\tilde{\tau} \leqslant \tilde{\tau}_c = 3.38$. Thus, we infer that for our choice of membrane parameters, stripe formation occurs only for $\gamma > 0.35$ nm^{-1}.

V. PATTERN FORMATION ON CURVED GEOMETRIES

We now consider the case where the substrate is not flat and instead has a uniform curvature γ_0. Without flipping, uniform substrate curvature has no effect on the lipid organization predicted by our model (see Appendix A). However, in the presence of flipping, we found that γ_0 acts as a chemical potential governing the compositional asymmetry of the two leaflets [Fig. 3(a)], which in turn impacts lipid organization and domain formation. At higher substrate curvatures, we observed increased prevalence of compact microdomains rather than stripes, due to greater asymmetry in the lipid A concentration [Figs. 3(b)–3(d)].

To mimic the geometry of rod-shaped bacteria, we used a lattice with higher substrate curvature at the leftmost and rightmost sixths, corresponding to the cell poles, and lower substrate curvature in between, representing the cylindrical midcell region. We carried out simulations of a 100×150 triangular lattice in which the polar regions had slightly increased substrate curvature of $\gamma_0 = 0.04$ nm^{-1} relative to midcell. We first considered a membrane with $\phi_{\text{out}} = 0$ (lipid A entirely in the inner leaflet) without flipping, and observed that for small γ, large domains formed that often localized to

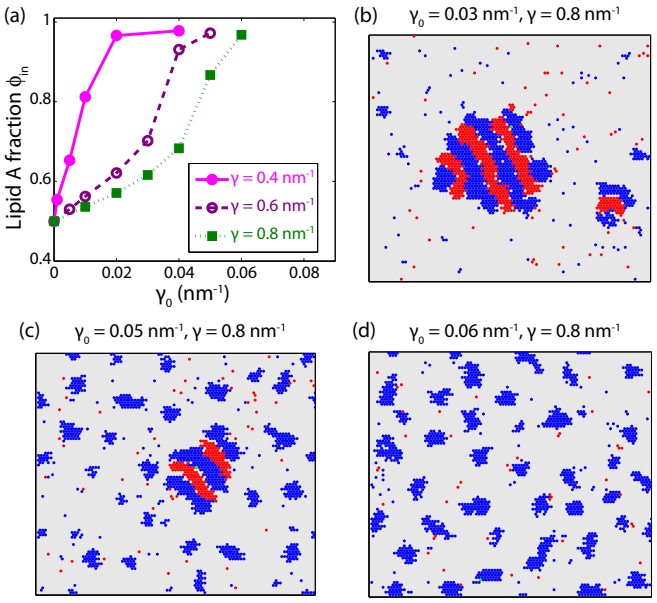

FIG. 3. Substrate curvature γ_0 inhibits stripe formation when lipids are free to flip between leaflets. (a) The lipid A fraction in the inner leaflet increases with increasing substrate curvature γ_0. (b–d) Typical equilibrated membrane configurations for various values of γ_0.

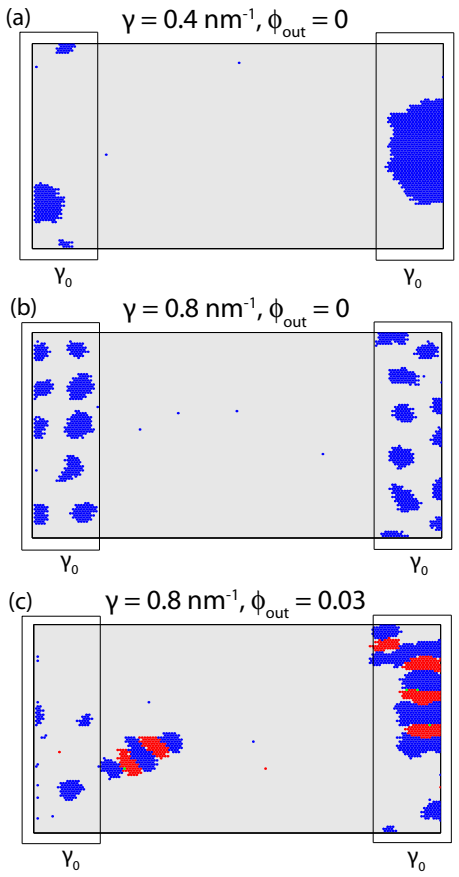

FIG. 4. Polar localization of domains of lipids with large intrinsic curvature requires low outer leaflet fraction. (a–c) Rectangles on the left and right represent bacterial cell poles with cell-wall curvature $\gamma_0 = 0.04$ nm^{-1}. $\phi_{in} = 0.075$ is fixed in all simulations. Shown are typical equilibrated membrane configurations for various values of γ and ϕ_{out}.

one of the poles [Fig. 4(a)]. Higher values of γ resulted in microdomains, that were distributed approximately equally at both poles [Fig. 4(b)]. Small increases in the lipid A fraction in the outer leaflet disturbed this localization, and above a threshold concentration bipolar localization was abolished [Fig. 4(c)]. The phase diagram in (γ, ϕ_{out}) space has microdomains with approximate equipartition between the poles for large values of γ and small ϕ_{out}, with a transition from bipolar to nonbipolar as γ is decreased or ϕ_{out} is increased. In the presence of lipid flipping, depending on our choice of parameter values, we typically found either striped domains without polar localization, or polar microdomains with average ϕ_{out} close to zero.

These results have important implications for the experimentally observed localization of cardiolipin to regions of higher curvature [8–10]. If there is little flipping between the leaflets, then our results imply that cardiolipin microdomains should distribute equally to the poles only for sufficiently asymmetric partitioning of cardiolipin between the two leaflets. However, if free flipping occurs, for appropriate choice of parameter values we can find most of the cardiolipin in the inner leaflet due to substrate curvature, leading to localization profiles that resemble the results from our previous modeling work [18,19], with polar localization except at very high or very low cardiolipin concentrations. We also note that the inner-leaflet localization of cardiolipin in the presence of flipping is tied to domain formation: namely, in the absence of domain formation the distribution of cardiolipin in the two leaflets would be similar due to the large difference between the size of individual cardiolpin molecules and the radius of the cell.

VI. CONCLUSIONS

In this study, we have demonstrated the rich capacity for pattern formation in pinned multicomponent lipid bilayers, which can exhibit both compact and striped domains depending on membrane biophysical properties and the composition of the two leaflets. These results may also be relevant to understanding the organization of membrane-associated proteins that are known to induce membrane curvature (see Ref. [16] for a review), such as coat-protein complexes, BAR domains, and cytoskeletal nucleation (formins, WASP, Arp2/3). Coupling of proteins to membrane curvature is relevant for many cellular processes, such as intracellular trafficking and cell motility. The basic ingredients of our model, particularly the interplay of composition-curvature coupling and phase separation (or, alternatively, membrane protein aggregation), are ubiquitous in geometric-sensing proteins. Thus, our proposed mechanism for spatial organization involving the interplay between short-range chemical interactions and longer-range elastic stresses is likely to be of widespread relevance for proteolipid organization in both prokaryotic and eukaryotic cells, as well as for *in vitro* supported bilayers.

ACKNOWLEDGMENTS

We acknowledge funding from NIH Grant No. R01 GM082938 and from NSF Grant No. PHY08-48550.

APPENDIX A: ENERGETICS OF THE MEMBRANE

The total energy of the membrane in our model is written as

$$E = E_{\text{elastic}} + E_{\text{int}}^{\text{in}} + E_{\text{int}}^{\text{out}}, \tag{A1}$$

where E_{elastic} represents the elastic energy of the membrane and $E_{\text{int}}^{\text{in/out}}$ represents the short range lipid-lipid interactions in the inner and outer leaflet. The interaction energies were discussed in Sec. II. The elastic energy is a sum of the bending energy of each leaflet and a pinning potential that penalizes deviation of the midplane of the membrane from a preferred height. The elastic energy of the membrane is given by

$$E_{\text{elastic}} = \int \left\{ \frac{\kappa}{4}[2H(\mathbf{r}) + \gamma_{\text{out}}(\mathbf{r})]^2 + \frac{\kappa}{4}[2H(\mathbf{r}) - \gamma_{\text{in}}(\mathbf{r})]^2 + \frac{\lambda}{2}[h(\mathbf{r}) - h_0(\mathbf{r})]^2 \right\} d\mathbf{r}, \tag{A2}$$

where H is the local mean curvature of the two-dimensional membrane, and $\gamma_{\text{in}}/\gamma_{\text{out}}$ is the composition-dependent local intrinsic curvature of the inner/outer leaflet, given by $\gamma_{\text{in/out}}(\mathbf{r}) = \gamma$ if there is a lipid A at $\mathbf{r}$ in the inner/outer leaflet, and $\gamma_{\text{in/out}} = 0$ if there is a lipid B at $\mathbf{r}$. The first two terms, proportional to bending stiffness κ, penalize the mismatch between the local mean curvature (H) of the membrane and the intrinsic curvature of the lipids ($\gamma_{\text{in/out}}$). In our model, we have assumed that the bending stiffness of both the inner and outer leaflet is equal and is half of the total bending modulus. The third term, proportional to the pinning modulus (λ), is the pinning potential that penalizes deformation of the membrane away from its preferred height (with $h(\mathbf{r})$ representing the local height of the membrane and $h_0(\mathbf{r})$ the preferred height). In the Monge representation, for small $\nabla h(\mathbf{r})$ the total mean curvature H can be approximated as $\nabla^2 h/2$, and the total elastic energy becomes

$$E_{\text{elastic}} = \int \left\{ \frac{\kappa}{4}[\nabla^2 h(\mathbf{r}) + \gamma_{\text{out}}(\mathbf{r})]^2 + \frac{\kappa}{4}[\nabla^2 h(\mathbf{r}) - \gamma_{\text{in}}(\mathbf{r})]^2 + \frac{\lambda}{2}[h(\mathbf{r}) - h_0(\mathbf{r})]^2 \right\} d\mathbf{r}. \tag{A3}$$

Defining $\tilde{h} = h - h_0$, we find that

$$E_{\text{elastic}} = \int \left\{ \frac{\kappa}{4}[\nabla^2 \tilde{h}(\mathbf{r}) + \gamma_0(\mathbf{r}) + \gamma_{\text{out}}(\mathbf{r})]^2 + \frac{\kappa}{4}[\nabla^2 \tilde{h}(\mathbf{r}) + \gamma_0(\mathbf{r}) - \gamma_{\text{in}}(\mathbf{r})]^2 + \frac{\lambda}{2}[\tilde{h}(\mathbf{r})]^2 \right\} d\mathbf{r}, \tag{A4}$$

where $\gamma_0 = \nabla^2 h_0(\mathbf{r})$ is the curvature of the substrate and for a flat substrate $\gamma_0 = 0$. The integral of $\kappa\gamma_{\text{in/out}}^2/4$ is independent of the membrane and substrate curvature and can be absorbed into the interaction energies ($E_{\text{int}}^{\text{in/out}}$). Moreover, we can discard the constant term $\kappa\gamma_0^2/2$, and rewrite the equation as

$$E_{\text{elastic}} = \int \left\{ \frac{\kappa}{2}[[\nabla^2 \tilde{h}(\mathbf{r})]^2 + [\gamma_{\text{out}}(\mathbf{r}) - \gamma_{\text{in}}(\mathbf{r})]\nabla^2 \tilde{h}(\mathbf{r}) + [\gamma_{\text{out}}(\mathbf{r}) - \gamma_{\text{in}}(\mathbf{r})]\gamma_0 + 2\gamma_0(\mathbf{r})\nabla^2 \tilde{h}(\mathbf{r})] + \frac{\lambda}{2}[\tilde{h}(\mathbf{r})]^2 \right\} d\mathbf{r}. \tag{A5}$$

For a membrane with uniform substrate curvature and fixed composition in each leaflet (no-flip case), the integral of the third term, $\int d\mathbf{r}[\gamma_{\text{out}}(\mathbf{r}) - \gamma_{\text{in}}(\mathbf{r})]\gamma_0$, gives a constant and can be ignored. However, if lipids are allowed to flip between the leaflets (free-flip case), γ_0 acts as a chemical potential, and the third term then controls the asymmetry of composition of the two leaflets. For uniform substrate curvature, the fourth term, $\sim\gamma_0 \int d\mathbf{r}\nabla^2 \tilde{h}(\mathbf{r})$, represents a boundary term and can be ignored. Thus in the no-flip case, since there are no remaining terms coupling γ_0 to the local composition, we find no dependence of pattern formation on substrate curvature (as mentioned in the main text).

For subsequent analysis of pattern formation, we set $\gamma_0 = 0$ (flat substrate), and introduce the fields $\phi(\mathbf{r})^{\text{in/out}}$ that represents the locally averaged fraction of lipid A at position $\mathbf{r}$ in the inner/outer leaflet. Defining $\phi(\mathbf{r}) = \phi(\mathbf{r})^{\text{in}} - \phi(\mathbf{r})^{\text{out}}$, we have $\langle\gamma_{\text{out}}(\mathbf{r}) - \gamma_{\text{in}}(\mathbf{r})\rangle_{\text{local}} = \gamma\phi(\mathbf{r})$. We rewrite E_{elastic} in Fourier space as

$$E_{\text{elastic}} = \frac{1}{2}\int \frac{1}{(2\pi)^2}\left\{ (\kappa q^4 + \lambda)|h_{\mathbf{q}}|^2 + \frac{\kappa\gamma q^2}{2}(\phi_{\mathbf{q}} h_{\text{q}}^* + \phi_{\mathbf{q}}^* h_{\mathbf{q}}) \right\} d\mathbf{q}, \tag{A6}$$

where $h_{\mathbf{q}}$ and $\phi_{\mathbf{q}}$ are 2D Fourier transforms of $h(\mathbf{r})$ and $\phi(\mathbf{r})$, respectively, specified, for example, as

$$h_{\mathbf{q}} = \int h(\mathbf{r}) e^{-i\mathbf{q}\cdot\mathbf{r}} d\mathbf{r}.$$

Here $q^2 = q_x^2 + q_y^2$, and $d\mathbf{q}$ refers to $dq_x dq_y$, where the range of integration for both q_x and q_y is $-\infty$ to ∞. We note that for a membrane with periodic boundary conditions of dimensions $L_x \times L_y$, we would have a double sum (instead of an integral) over all allowed values of q_x (of the form $2\pi n_x/L_x$, where n_x is an integer) and q_y (of the form $2\pi n_y/L_y$, where n_y is an integer). In the thermodynamic limit where $L_x, L_y \to \infty$, the double sum can be replaced by the double integral used in Eq. (A6). Using the relation

$$c_1|h|^2 + c_2(\phi^* h + \phi h^*) = c_1\left|h + \frac{c_2}{c_1}\phi\right|^2 - \frac{c_2^2}{c_1}|\phi|^2,$$

we can then write

$$E_{\text{elastic}} = \frac{1}{2}\int \frac{1}{(2\pi)^2}\left\{ (\kappa q^4 + \lambda)\left|h_{\mathbf{q}} + \frac{\kappa\gamma q^2}{2(\lambda + \kappa q^4)}\phi_{\mathbf{q}}\right|^2 - \frac{\kappa^2\gamma^2 q^4}{4(\lambda + \kappa q^4)}|\phi_{\mathbf{q}}|^2 \right\} d\mathbf{q}. \tag{A7}$$

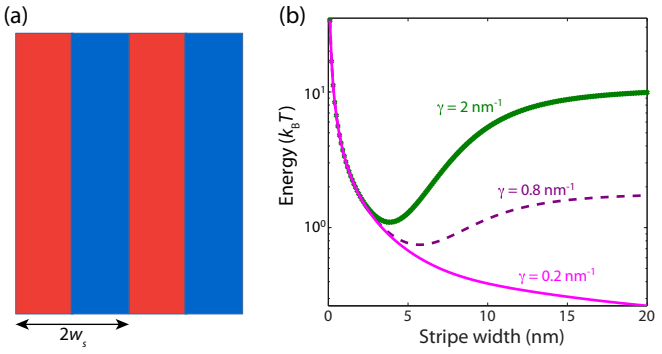

FIG. 5. (a) Schematic showing stripes of conical lipid in the inner (blue) and outer (red) leaflet of a bilayer. (b) Energy of the bilayer calculated using Eq. (B6) versus stripe width (w_s) for estimated line tension $\tau = 1.68\, k_BT\text{nm}^{-1}$ and different intrinsic curvatures γ.

Carrying out the trace over $\{h\}$, we are left only with the last term in Eq. (A7), which can be written as

$$E_{\text{elastic}} = -\frac{\kappa\gamma^2}{8}\int \frac{1}{(2\pi)^2}\left(|\phi_{\mathbf{q}}|^2 - \frac{\lambda}{\lambda+\kappa q^4}|\phi_{\mathbf{q}}|^2\right)d\mathbf{q}. \tag{A8}$$

For a membrane with fixed composition in both inner and outer leaflets and having alternating stripes of lipids with intrinsic curvature, the first term gives a constant and can be ignored. Then Eq. (A8) reduces to

$$E_{\text{elastic}} = \frac{\kappa\lambda\gamma^2}{8}\int \frac{1}{(2\pi)^2}\frac{1}{\lambda+\kappa q^4}|\phi_{\mathbf{q}}|^2 d\mathbf{q}. \tag{A9}$$

In real space, this can be written in the convolution form

$$E_{\text{elastic}} = \frac{1}{2}\int V(\mathbf{r}-\mathbf{r}')\phi(\mathbf{r})\phi(\mathbf{r}')d\mathbf{r}d\mathbf{r}', \tag{A10}$$

where $V(\mathbf{r}-\mathbf{r}')$ is an effective repulsive potential, identical to the elastic potential discussed in Ref. [19]. If we consider interactions between lipid A molecules present in the same leaflet, say the inner leaflet, then we can replace $\phi(\mathbf{r})$ by $\phi(\mathbf{r})^{\text{in}}$ and obtain an effective repulsion between lipid A molecules. However, for interactions between lipid A molecules on opposite leaflets, the elastic energy takes the form $-\int d\mathbf{r}d\mathbf{r}' V(\mathbf{r}-\mathbf{r}')\phi(\mathbf{r})^{\text{out}}\phi(\mathbf{r}')^{\text{in}}$, which corresponds to an effective attractive interaction. This result assumed lipid A molecules in opposite leaflets do not overlap in their lateral position; overlapping of lipid A molecules would correspond to an energy cost due to curvature frustration.

APPENDIX B: ANALYTICAL CALCULATION OF STRIPE WIDTH

To estimate the stripe width analytically, consider a flat membrane of width L_x and height L_y, where we will assume the thermodynamic limit $L_x, L_y \to \infty$. We also assume for simplicity that the stripes are perfect rectangles of width w_s as shown in Fig. 5(a), and alternate in the two leaflets: red (lighter gray in print version) and blue (darker gray in print version). The elastic energy of the membrane is given by [Eq. (A9)]

$$E_{\text{elastic}} = \frac{\kappa\lambda\gamma^2}{8}\int \frac{1}{(2\pi)^2}\frac{1}{\lambda+\kappa q^4}|\phi_{\mathbf{q}}|^2 d\mathbf{q}. \tag{B1}$$

For a membrane with perfect stripes parallel to the vertical axis, $\phi(\mathbf{r})$ depends only on the coordinate x and is periodic with a period of $2w_s$. $\phi(\mathbf{r})$ can be written as

$$\begin{aligned}\phi(\mathbf{r}) = \phi(x) = {} & 1,\ 0 < x < w_s \text{ (conical lipids in outer layer)},\\ & -1,\ w_s < x < 2w_s \text{ (conical lipids in inner layer)},\end{aligned} \tag{B2}$$

and hence can be written as a Fourier series

$$\phi(x) = \frac{4}{\pi}\sum_{n=\text{odd}}\frac{\sin(n\pi x/w_s)}{n}, \tag{B3}$$

where the sum is over positive odd integer values of n. The Fourier transform of $\phi(\mathbf{r})$ is given by

$$\begin{aligned}\phi_{\mathbf{q}} &= \int \phi(\mathbf{r})e^{-i\mathbf{q}\cdot\mathbf{r}}d\mathbf{r}\\ &= \int \phi(x)e^{-i(q_x x+q_y y)}dxdy\\ &= 2\pi\delta(q_y)\sum_{n=\text{odd}}\int \frac{4}{n\pi}\sin\left(\frac{n\pi x}{w_s}\right)e^{-iq_x x}dx\\ &= 2\pi\delta(q_y)\sum_{n=\text{odd}}\frac{4}{n\pi}\frac{\pi}{i}\left[\delta\left(q_x+\frac{n\pi}{w_s}\right)-\delta\left(q_x-\frac{n\pi}{w_s}\right)\right]\\ &= 8\pi\delta(q_y)\sum_{n=\text{odd}}\frac{i}{n}\left[\delta\left(q_x-\frac{n\pi}{w_s}\right)-\delta\left(q_x+\frac{n\pi}{w_s}\right)\right].\end{aligned}$$

Note that in the above expression, we treat the Dirac δ function $\delta(q_y)$ as equivalent to $(L_y/2\pi)\delta_{q_y,0}$ in the limit $L_y \to \infty$, where $\delta_{q_y,0}$ is the Kronecker δ function. Substituting for $\phi_{\mathbf{q}}$ in Eq. (B1) we obtain

$$E_{\text{elastic}} = 2\kappa\lambda\gamma^2\sum_{n,n'=\text{odd}}\int \frac{1}{\lambda+\kappa q^4}\frac{[\delta(q_y)]^2}{nn'}\left[\delta\left(q_x-\frac{n\pi}{w_s}\right)-\delta\left(q_x+\frac{n\pi}{w_s}\right)\right]\left[\delta\left(q_x-\frac{n'\pi}{w_s}\right)-\delta\left(q_x+\frac{n'\pi}{w_s}\right)\right]d\mathbf{q}. \tag{B4}$$

These results can also be obtained by using well known properties of the Dirac δ function combined with the finite equivalence given above.

Integration over dq_y gives

$$\int_{-\infty}^{\infty}\frac{[\delta(q_y)]^2}{\lambda+\kappa\left(q_x^2+q_y^2\right)^2}dq_y = \frac{1}{\lambda+\kappa q_x^4}\delta(q_y=0) = \frac{L_y}{2\pi\left(\lambda+\kappa q_x^4\right)},$$

where we have replaced $\delta(q_y)$ by $(L_y/2\pi)\delta_{q_y,0}$ for the last equality. Equation (B4) then reduces to

$$\begin{aligned}
E_{\text{elastic}} &= \frac{\kappa\lambda\gamma^2}{\pi}\sum_{n,n'=\text{odd}}\int_{-\infty}^{\infty}\frac{L_y}{\lambda+\kappa q_x^4}\frac{1}{nn'}\left[\delta\left(q_x-\frac{n\pi}{w_s}\right)-\delta\left(q_x+\frac{n\pi}{w_s}\right)\right]\times\left[\delta\left(q_x-\frac{n'\pi}{w_s}\right)-\delta\left(q_x+\frac{n'\pi}{w_s}\right)\right]dq_x \\
&= \frac{\kappa\lambda\gamma^2}{\pi}\sum_{n,n'=\text{odd}}\int_{-\infty}^{\infty}\frac{L_y}{\lambda+\kappa q_x^4}\frac{1}{nn'}\left[\delta\left(q_x-\frac{n\pi}{w_s}\right)\delta\left(q_x-\frac{n'\pi}{w_s}\right)-\delta\left(q_x-\frac{n\pi}{w_s}\right)\delta\left(q_x+\frac{n'\pi}{w_s}\right)\right. \\
&\quad\left.-\delta\left(q_x+\frac{n\pi}{w_s}\right)\delta\left(q_x-\frac{n'\pi}{w_s}\right)+\delta\left(q_x+\frac{n\pi}{w_s}\right)\delta\left(q_x+\frac{n'\pi}{w_s}\right)\right]dq_x \\
&= \frac{\kappa\lambda\gamma^2}{\pi}\sum_{n,n'=\text{odd}}\frac{L_y}{\lambda+\kappa\left(\frac{n\pi}{w_s}\right)^4}\frac{1}{nn'}\frac{L_x}{2\pi}[\delta_{n,n'}-\delta_{n,-n'}-\delta_{-n,n'}+\delta_{n,n'}],
\end{aligned}$$

where we have once again utilized the equivalence between the Dirac δ function and $L_x/(2\pi)$ times the Kronecker δ function, valid in limit $L_x\to\infty$, for the last equality. The second and third terms vanish since n, n' are positive odd numbers, while the first and last terms only contribute when $n = n'$. Thus,

$$E_{\text{elastic}} = \frac{\lambda\gamma^2}{\pi^2}\sum_{n=\text{odd}}\frac{L_yL_xd^4}{\frac{\lambda}{\kappa}w_s^4+(n\pi)^4}\frac{1}{n^2},$$

$$\frac{E_{\text{elastic}}}{A} = \frac{\lambda\gamma^2}{\pi^2}\sum_{n=\text{odd}}\frac{w_s^4}{\frac{\lambda}{\kappa}w_s^4+(n\pi)^4}\frac{1}{n^2},$$

where $A = L_xL_y$ is the area of the membrane. The energy per unit area due to line tension (τ) for the system is given by

$$\frac{E_{\text{int}}}{A} = \frac{4\tau L_y}{L_y 2w_s} = \frac{2\tau}{w_s}. \tag{B5}$$

The total energy per unit area for the system is

$$E_{\text{total}} = \frac{\lambda\gamma^2}{\pi^2}\sum_{n=\text{odd}}\frac{w_s^4}{\frac{\lambda}{\kappa}w_s^4+(n\pi)^4}\frac{1}{n^2}+\frac{2\tau}{w_s}. \tag{B6}$$

The optimum stripe width is found by minimizing E_{total} for given values of membrane parameters (γ,κ,λ). In Eq. (B6), τ is a fitting parameter that was estimated by performing a least-squares fit of the stripe width obtained by simulations for various values of intrinsic curvature (γ). In Fig. 5(b), we have plotted E_{total} versus d for $\tau = 1.68\,k_BT\,\text{nm}^{-1}$ and different values of intrinsic curvature γ. For $\gamma = 2\,\text{nm}^{-1}$, we obtain a well defined minimum in the curve, confirming the presence of stripes of width 3.85 nm. For the very small value of $\gamma = 0.2\,\text{nm}^{-1}$ we do not find any minimum in the curve. This implies that below a critical value of γ, the membrane minimizes its energy by forming macrodomains, rather than alternating stripes in the two leaflets.

Substituting $\alpha = (\kappa/\lambda)^{1/4}$ in Eq. (B6), we obtain

$$\tilde{E} = \sum_{n=\text{odd}}\frac{\tilde{d}^4}{\tilde{w}_s^4+(n\pi)^4}\frac{1}{n^2}+\frac{\tilde{\tau}}{\tilde{w}_s}, \tag{B7}$$

where $\tilde{E} = \pi^2E_{\text{total}}/\kappa\gamma^2$, $\tilde{w}_s = w_s/\alpha$ and $\tilde{\tau} = 2\pi^2\tau/\alpha\kappa\gamma^2$ are dimensionless energy, stripe width, and line tension, respectively. For a given value of $\tilde{\tau}$, the scaled stripe width is obtained by minimizing the scaled energy $\tilde{E}$. Thus the scaled stripe width, $\tilde{w}_s$, depends only on a single parameter, namely the scaled line tension $\tilde{\tau}$.

APPENDIX C: SIMULATION METHODOLOGY

We represent the membrane as a two-dimensional triangular lattice with lattice spacing $a = 1$ nm, fully occupied by lipids of type A or B. To account for the two leaflets, we assume each lattice site is occupied by two distinct lipids, one in the inner and the other in the outer leaflet. In a lattice model, the membrane energy can be written as $E = E_{\text{elastic}} + E_{\text{int}}$, where the elastic energy given by Eq. (A5) in the main text (the last term, which is independent of h, is absorbed in the interaction energies) can be written as

$$\begin{aligned}
E_{\text{elastic}} = A\sum_i\left(\frac{\kappa}{2a^4}\left[4h_i-\zeta\sum_{\text{nn.:}j}h_j\right]^2\right. \\
\left.+\frac{\kappa\gamma}{2a^2}\sigma_i\left[4h_i-\zeta\sum_{\text{nn:}j}h_j\right]+\frac{\lambda}{2}h_i^2\right),
\end{aligned} \tag{C1}$$

where h_i is the height of the membrane at lattice site i, and $\sigma_i = 2\gamma_0/\gamma + 1$ if there is a lipid A in the outer leaflet and B in the inner, $2\gamma_0/\gamma$ if there is lipid A or lipid B in both the leaflets, and $2\gamma_0/\gamma - 1$ if there is lipid A in the inner leaflet and B in outer, with $\gamma_0 = 0$ for the case of a flat substrate. The innermost sum is over the nearest neighbors j of the lattice site i, and the prefactor ζ is 2/3 for a triangular lattice [19]. For a triangular lattice, the area per lipid, A, is $\sqrt{3}/2\,\text{nm}^2$.

The membrane elastic energy can be written in matrix form as

$$E_{\text{elastic}} = \frac{1}{2}\sum_{ij}h_iS_{ij}h_j+\sum_i h_iT_i, \tag{C2}$$

where $\mathbf{S}$ is a real, symmetric matrix that does not depend on the lipid variable σ_i and

$$T_i = \frac{\kappa\gamma}{2a^2}\left(4\sigma_i-\sum_{\text{nn:}j}\sigma_j\right). \tag{C3}$$

In Dirac notation, we can rewrite Eq. (C2) as

$$E_{\text{elastic}} = \tfrac{1}{2}\langle h|\mathbf{S}|h\rangle+\langle h|T\rangle. \tag{C4}$$

In our simulation, we first minimize the membrane energy with respect to the height field h_i, which gives $\sum_i S_{ij}h_j =$

$-T_i$ or $\mathbf{S}|h\rangle = -|T\rangle$, and hence $|h\rangle = -\mathbf{S}^{-1}|T\rangle$, thus

$$\min(E_{\text{elastic}}) = -\frac{1}{2}\langle T|\mathbf{S}^{-1}|T\rangle = -\frac{1}{2}\sum_{ij} T_i S_{ij}^{-1} T_j. \quad \text{(C5)}$$

Since the matrix $\mathbf{S}$ does not depend on the lipid type variable σ_i, $\mathbf{S}^{-1}$ has to be calculated only once, whereas T must be updated every time σ_i changes.

We performed Metropolis Monte Carlo simulations to minimize the total membrane energy for both flat substrates and substrates with spatially varying background curvature (γ_0). In our simulations we considered both the cases where the lipid composition in each leaflet is fixed (no-flip) as well as systems in which lipids from one leaflet can flip to the other (free-flip). Randomly selected pairs of unlike lipids are exchanged with probability $\min\{1, \exp[(E_i - E_f)/k_B T]\}$, where E_i and E_f are the total membrane energy before and after the move, respectively, until the distribution of lipid domain sizes reaches steady state. In the first case of fixed composition of each leaflet, the lipid pairs have to be selected from the same leaflet, while in the second case pairs are chosen at random either from the same or different leaflets. For the simulations we have assumed a fixed value for the membrane stiffness modulus $\kappa = 25\,k_B T$ and, unless otherwise specified, a pinning modulus $\lambda = 0.25\,k_B T\,\text{nm}^{-4}$.

APPENDIX D: EFFECT OF PINNING POTENTIAL ON STRIPE WIDTH

Based on the dependence of the scaled stripe width on the scaled line tension, we can deduce how stripe width depends on the cardiolipin intrinsic curvature (γ), line tension, and pinning potential. Here we focus on the effect of pinning potential on stripe width. For this purpose, we simulated the membrane with lipid parameters ($\kappa = 25\,k_B T$, $\varepsilon_{AB} = 1\,k_B T$, $\gamma = 0.4$ and $0.8\ \text{nm}^{-1}$) and varying pinning potentials (in the case of a bacterial membrane the pinning potential can in principle be varied by changing the osmotic pressure difference across the membrane). The stripe width is obtained from the Fourier transform of the images. We found that

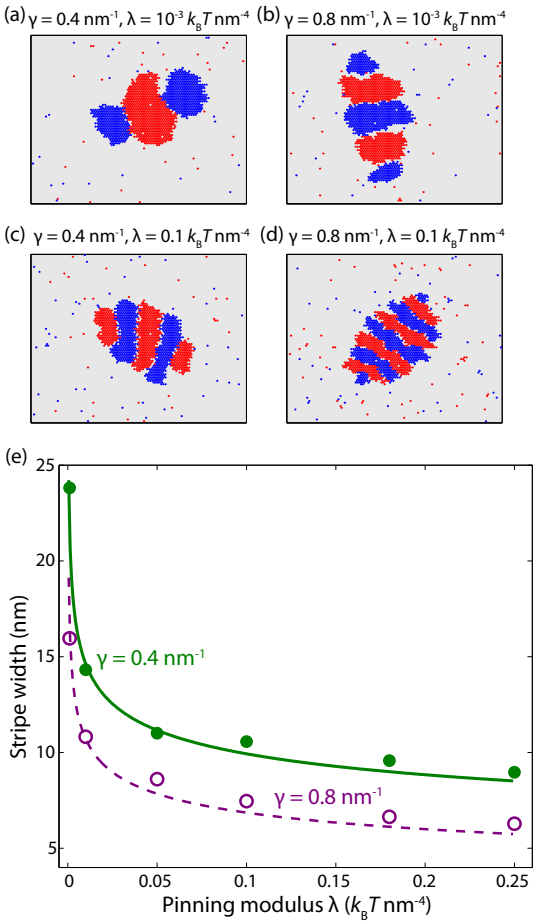

FIG. 6. Effect of pinning potential λ on stripe width. (a–d) Membrane configurations for $\gamma = 0.4\ \text{nm}^{-1}$ (left) and $0.8\ \text{nm}^{-1}$ (right) for $\lambda = 0.001\,k_B T\ \text{nm}^{-4}$ (top) and $0.1\,k_B T\,\text{nm}^{-4}$ (bottom). (e) Variation of stripe width calculated analytically (solid and dashed curves) for line tension $\tau = 1.68\,k_B T\,\text{nm}^{-1}$ and obtained by simulation (filled and open circles).

for both $\gamma = 0.4$ and $0.8\ \text{nm}^{-1}$ the stripe width decrease with increasing pinning potential as expected (Fig. 6). We compared the results of our simulations with our analytical calculations, as described in the previous section, with line tension set to $\tau = 1.68\,k_B T\,\text{nm}^{-1}$ and found good agreement [Fig. 6(e)].

[1] K. Simons and W. L. C. Vaz, Annu. Rev. Biophys. Biomol. Struct. **33**, 269 (2004).
[2] R. Parthasarathy and J. T. Groves, Soft Matt. **3**, 24 (2007).
[3] R. Phillips, T. Ursell, P. Wiggins, and P. Sens, Nature **459**, 379 (2009).
[4] N. S. Wingreen and K. C. Huang, Annu. Rev. Microbiol. **69**, 361 (2015).
[5] J. Lutkenhaus, Curr. Opin. Microbiol. **5**, 548 (2002).
[6] L. Shapiro, H. L. McAdams, and R. Losick, Science **298**, 1942 (2002).
[7] D. Lopez, Chem. Phys. Lipids **192**, 3 (2015).
[8] E. Mileykovskaya and W. Dowhan, J. Bacteriol. **182**, 1172 (2000).
[9] C. M. Koppelman, T. den Blaauwen, M. C. Duursma, R. M. A. Heeren, and N. Nanninga, J. Bacteriol. **183**, 6144 (2001).
[10] F. Kawai, M. Shoda, R. Harashima, Y. Sadaie, H. Hara, and K. Matsumoto, J. Bacteriol. **186**, 1475 (2004).
[11] L. D. Renner and D. B. Weibel, Proc. Natl. Acad. Sci. U.S.A. **108**, 6264 (2011).
[12] D. Lingwood and K. Simons, Science **327**, 46 (2010).
[13] M. Edidin, Annu. Rev. Biophys. Biomol. Struct. **32**, 257 (2003).

[14] K. Gauss, E. Gratton, E. P. W. Kable, A. S. Jones, I. Gelissen, L. Kritharides, and W. Jessup, Proc. Natl. Acad. Sci. U.S.A. **100**, 15554 (2003).
[15] M. Tanaka and E. Sackmann, Nature **437**, 656 (2005).
[16] R. Parthasarathy, C. H. Yu, and J. T. Groves, Langmuir **22**, 5095 (2006).
[17] J. T. Groves, Annu. Rev. Phys. Chem. **58**, 697 (2007).
[18] K. C. Huang, R. Mukhopadhyay, and N. S. Wingreen, PLoS Comput. Biol. **2**, e151 (2006).
[19] R. Mukhopadhyay, K. C. Huang, and N. S. Wingreen, Biophys. J. **95**, 1034 (2008).
[20] T. Romantsov, S. Helbig, D. E. Culham, C. Gill, L. Stalker, and Janet M. Wood, Mol. Micro. **64**, 1455 (2007).
[21] R. D. Kornberg and H. M. McConnell, Biochemistry **10**, 1111 (1971).
[22] W. C. Wimley and T. E. Thompson, Biochemistry **29**, 1296 (1990).
[23] T. Pomorski, S. Hrafnsdottir, P. F. Devauxb, and Gv. Meera, Sem. Cell Dev. Biol. **12**, 139 (2001).
[24] S. Rozovsky, Y. Kaizuka, and J. T. Groves, J. Am. Chem. Soc. **127**, 36 (2005).
[25] U. Seifert, Adv. Phys. **46**, 13 (1997).
[26] T. Pilizota and J. W. Shaevitz, Biophys. J. **104**, 2733 (2013).
[27] G. R. Chichili and W. Rodgers, Cell. Mol. Life Sci. **66**, 2319 (2009).
[28] N. Gov, A. G. Zilman, and S. Safran, Phys. Rev. Lett. **90**, 228101 (2003).
[29] C. M. Funkhouser, F. J. Solis, and K. Thornton, J. Chem. Phys. **138**, 024909 (2013).
[30] S. F. Shimobayashi, M. Ichikawa, and T. Taniguchi, Europhys. Lett. **113**, 56005 (2016).
[31] T. Baumgart, S. T. Hess, and W. W. Webb, Nature **425**, 821 (2003).